LBL-14857
c.2

Lawrence Berkeley Laboratory
UNIVERSITY OF CALIFORNIA

Materials & Molecular Research Division

To be published in the American Institute of Physics Conference Proceedings for the International Conference on X-Ray and Atomic Inner-Shell Physics, University of Oregon, Eugene, OR, August 23-27, 1982

RESONANCE AND THRESHOLD EFFECTS IN PHOTOEMISSION UP TO 3500 eV

D.A. Shirley, P.H. Kobrin, D.W. Lindle, C.M. Truesdale, S.H. Southworth, U. Becker and H.G. Kerkhoff

August 1982

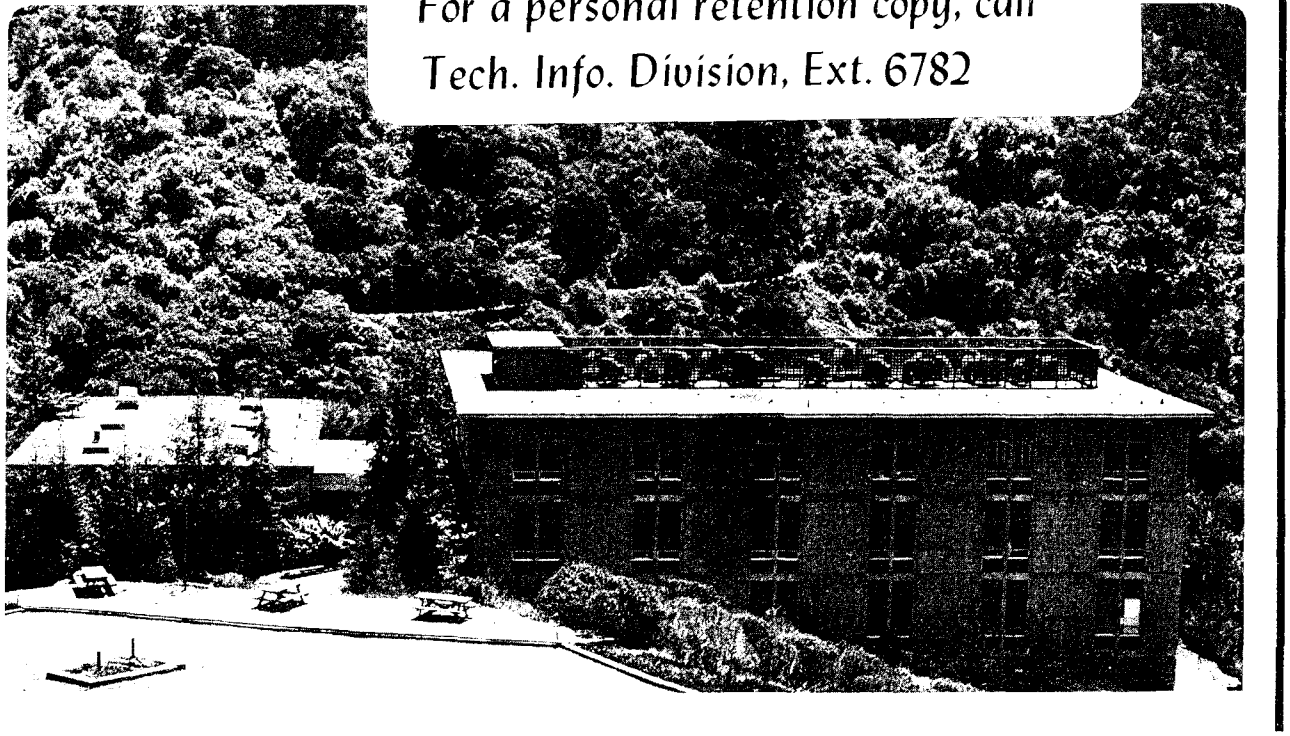

Prepared for the U.S. Department of Energy under Contract DE-AC03-76SF00098

LBL-14857

RESONANCE AND THRESHOLD EFFECTS IN PHOTOEMISSION UP TO 3500 eV*

D.A. Shirley, P.H. Kobrin, D.W. Lindle, C.M. Truesdale,
and S.H. Southworth †
Materials and Molecular Research Division
Lawrence Berkeley Laboratory
and
Department of Chemistry
University of California
Berkeley, California 94720

U. Becker and H.G. Kerkhoff
Technische Universität Berlin,
Fachbereich Physik,
Berlin, West Germany

ABSTRACT

Beam Lines at the Stanford Synchrotron Radiation Laboratory (SSRL) now provide photon beams throughout the entire energy range 5-5000 eV, with a pulse structure very well-suited to time-of-flight (TOF) photoelectron spectroscopy. We have used this facility, together with a TOF spectrometer, to measure photoemission cross sections $\sigma(\varepsilon)$ and asymmetry parameters $\beta(\varepsilon)$ for several interesting systems. A summary of early results is given.

Metal vapors (Ba, Cd, Mn, Hg) were studied using a high-temperature oven. Resonant photoemission was observed in several cases. Both $\sigma(\varepsilon)$ and $\beta(\varepsilon)$ showed resonant behavior at 21.1 eV for several lines in Cd. The 4d, 5s, and 5p $\sigma(\varepsilon)$ line profiles differed dramatically, illustrating the detailed information about continuum states that is available from photoemission.

Correlation satellites in photoemission from rare gases have been observed over a very wide energy range, including those seen in the K-shells of He, Ne and Ar and in the L-shell of Ne. The structure and preliminary intensity variations of these satellites will be discussed.

Molecular shape resonances in C(1s), N(1s), and O(1s) photoemission were observed for the first time, in the molecules CO, CO_2, OCS, CF_4, N_2 and NO. Both the π and σ resonances were observed in KVV Auger emission, and the σ resonances were studied by photoemission. The asymmetry parameters were measured in all cases. The results are in fair agreement with theory, but show systematic deviations and trends.

INTRODUCTION

Over the last four and one-half years, our group has been involved in gas-phase photoelectron spectroscopy using synchrotron radiation at the Stanford Synchrotron Radiation Laboratory

(SSRL). We have used three beam lines at SSRL which together span the photon energy range 5 to 4000 eV: The 8° line, which uses a Seya-Namioka monochromator, up to ~32 eV; the new 4° line, a grasshopper monochromator, from 25 to 600 eV; and the 2° line, which has a double-crystal monochromator with interchangable crystals, between 800 and 4000 eV.

The pulsed light through each of the monochromators is used to measure the kinetic energy spectrum of photoelectrons by the time-of-flight (TOF) method. This method of energy analysis is feasible at SSRL because of the large circumference of the SPEAR storage ring, which provides SSRL with photon pulses separated by as much as 780 nsec. The advantage of measuring the time spectrum is that all photoelectron energies are sampled simultaneously, making the analyzer more efficient than a scanning deflection analyzer.

The differential cross section for emission of photoelectrons from a randomly oriented sample by linearly polarized light into a given solid angle, Ω, is given by

$$\frac{d\sigma}{d\Omega} = \frac{\sigma(\varepsilon)}{4\pi}\left(1 + \beta(\varepsilon)P_2(\cos\theta)\right), \qquad (1)$$

where θ is the angle between the polarization of the light and the momentum of the photoelectron, $\sigma(\varepsilon)$ is the energy dependent total cross section, $\beta(\varepsilon)$ is the energy dependent angular distribution asymmetry parameter, and $P_2(\cos\theta)$ is the second Legendre polynomial. To measure $\sigma(\varepsilon)$, we use a TOF analyzer positioned at θ=54.7°, the "magic angle", where $P_2(\cos\theta)$=0. In order to determine $\beta(\varepsilon)$, we need only measure $d\sigma/d\Omega$ at one other angle. This scheme is known as the double-angle time-of-flight (DATOF) method and is schematically represented in Fig. 1 and described in Refs. 1 and 2.

There is an additional advantage to the DATOF method besides the collection efficiency. When measuring a branching ratio, which is the ratio of two peak areas in the magic-angle detector, or a $\beta(\varepsilon)$, which is the ratio of two peak areas, one from each detector, the sample pressure, photon flux and even the collection time are unimportant. Thus, the pressure and photon flux do not need to be monitored except to compare cross sections at different photon energies.

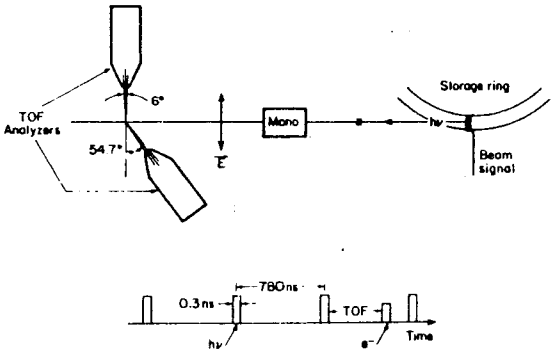

Fig. 1. Schematic of the Double-Angle Time-of-Flight (DATOF) method.

We have used our

apparatus to probe several interesting systems, some of which are described in this paper. A resistively heated oven has been built to produce metal vapor beams of Ba, Cd, Mn, and Hg. These metal vapor experiments are described in Sec. II. The efficiency of the TOF method was utilized in several experiments on low intensity satellite lines in He, Ne and Ar which are described in Sec. III. The ability to measure angular distributions at the C, N, and O K-edges was used to observe shape resonances from small molecules. These experiments are discussed in Sec. IV. Sec. V describes recent work on CH_3I as a molecular analog to our previous study of the Xe 4d subshell. Conclusions are presented in Sec. VI.

METAL VAPOR EXPERIMENTS

Our research group has had an historic interest in the photoemission of metal vapors. These early electron correlation studies were based upon the Perkin-Elmer PS-18 Photoelectron Spectrometer, which was used to investigate mostly group IIA, group IIB and lanthanide elements at the HeI and NeI line source energies. This work led us to the use of synchrotron radiation and the study of resonant photoemission.

Fig. 2 shows the total electron yield from atomic Ba. We see that there are several strong absorption features which are due to discrete states of neutral Ba embedded in the ion plus electron continuum. To examine these resonances further, the photon energy was tuned to the two photon energies that have been

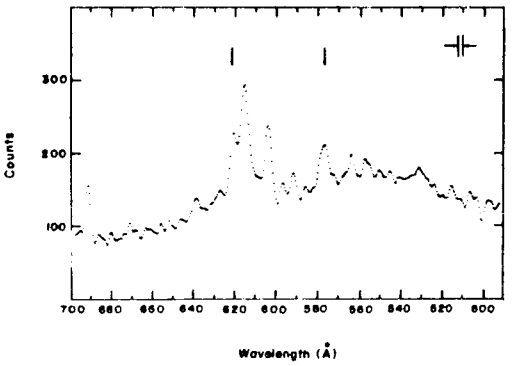

Fig. 2. Total electron yield spectrum of atomic Ba.

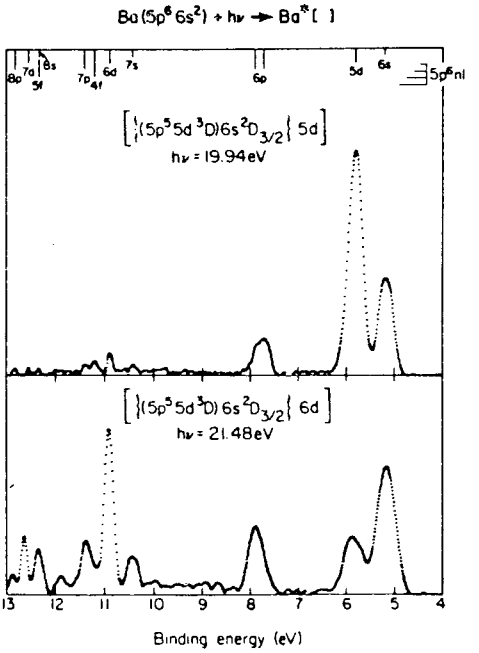

Fig. 3. Photoelectron spectra of atomic Ba taken at two autoionizing resonances.

denoted by arrows in Fig. 2. These two photoelectron spectra are shown in Fig. 3. A direct photoemission spectrum would show the 6s photoelectron peak to be the largest, yet at 19.94 eV the 5d peak is the largest, and at 21.48 eV the 6d peak is greatly enhanced. These enhancements are a fingerprint of the autoionizing states that are excited and illustrate the utility of the resonance photoemission method. The nature of the decay can be interpreted in terms of an "Auger decay" model in which the excited nd electron acts as a spectator to the Coster-Kronig transition $5p^5 5d6s \rightarrow 5p^6 + e^-$.[3]

It is well known that absorption features above the first ionization threshold are not always lorentzian as are those of Ba in Fig. 2. In fact, it has been shown by Fano that the interference between direct photoemission and photoexcitation followed by autoionizing decay can lead to a family of absorption shapes now known as Fano profiles.[4] These profiles have the form

$$\sigma(\varepsilon) = \sigma_t \left[\rho^2 \frac{2(q+\varepsilon)^2}{1+\varepsilon^2} + 1-\rho^2 \right] \qquad (2)$$

where ε is a reduced energy equal to $2(E-E_0)/\Gamma$, E_0 is the resonance position, Γ its width, σ_t is the cross section away from the resonance, and q and ρ^2 are constants. While Eq. (2) gives the shape of the total absorption or total electron emission, we may ask what the shapes of the partial cross section profiles for each photoelectron peak are.

To answer this question we looked at the broad autoionizing resonance in Cd I at 21.1 eV. Photoelectron spectra were taken over this asymmetric resonance, and the partial cross section for producing each of the final ionic states was determined. These partial cross sections are shown in Figs. 4 and 5. We find that the partial cross section profiles differ dramatically at this resonance. These different shapes can be understood by considering the details of the autoionization. A theoretical formalism developed by Starace[5] and by Davis and Feldkamp[6] has been applied to this system and parameters have been extracted.[7].

The absorption spectrum of Mn I is dominated by a "giant resonance" near 50 eV which is based upon a $3p \rightarrow 3d$ transition into the half-filled 3d shell. Resonant photoemission from Mn shows that several ionic states are populated from the autoionizing state. In addition to the main $3d^{-1}$ line, there are several two-electron satellites with a 3d hole. These satellites show enhancements at the giant resonance and also at the 3p threshold 5 eV higher. The nature of the enhancement at the 3p threshold is interesting in that the main $3d^{-1}$ line does not undergo a corresponding enhancement.

In addition to the above mentioned resonant work, we have

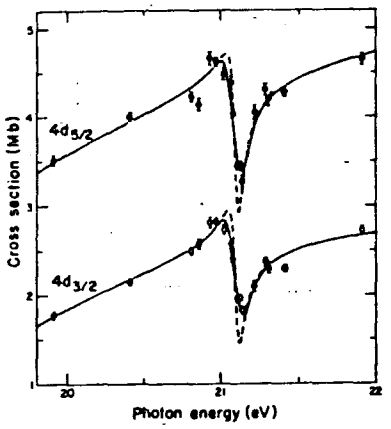

Fig. 4

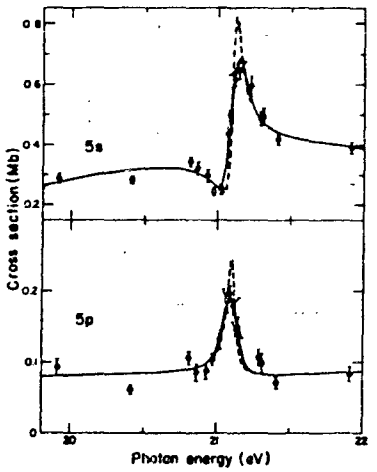

Fig. 5

Fig. 4. Partial cross section measurements of the $3d^9 4s^2\ ^2D_{5/2}$ (filled circles), and $3d^9 4s^2\ ^2D_{3/2}$ (open circles), photoelectrons. The solid curves are fits to a theoretical lineshape convoluted with the monochromator bandpass. Dashed curves show fits with monochromator broadening removed.

Fig. 5. Same as Fig. 4, except for $3d^{10}4s\ ^2S_{1/2}$ and $3d^{10}4p\ ^2P_{3/2,1/2}$ photoelectrons.

studied the photoionization of Hg. Because of its high atomic number, we expect both relativistic and many body effects to be important in Hg. We measured the relative cross sections, subshell branching ratios and angular distributions of the 5d, 5p and 4f subshells between 50 and 275 eV.

Fig. 6 shows the angular distribution asymmetry parameter for the 5d photoelectron and a calculation using the RRPA theory. The RRPA calculation includes intershell correlations with the 4f and 5p channels as well as relativistic effects. The drop in $\beta(\varepsilon)$ near 190 eV is caused by a Cooper minimum in the $5d \rightarrow \varepsilon f$ channel.

Fig. 7 shows the asymmetry parameter of the 4f subshell. The cross section and branching ratio as well as the $\beta(\varepsilon)$ parameter show the effects of a large centrifugal barrier near threshold in the $4f \rightarrow \varepsilon g$ channel.

The $5p_{3/2}$ and $5p_{1/2}$ photoionization channels show large variations in all of the measurable parameters due to a large spin-orbit splitting (18.6 eV) and a Cooper minimum 100 eV above threshold.

These experiments with metal vapors highlight the advantages of the DATOF method: the insensitivity of the branching ratio and angular distribution measurements to the sample pressure and photon flux.

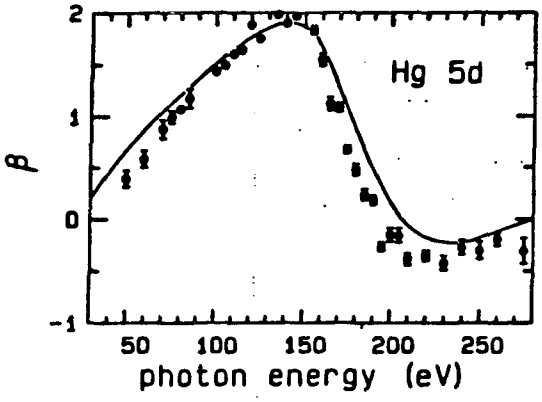

Fig. 6

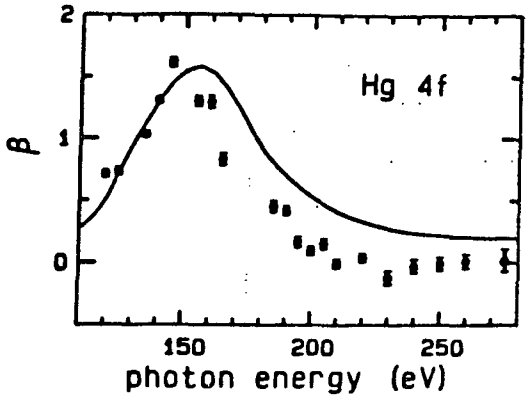

Fig. 7

Fig. 6. Angular distribution asymmetry parameter of the Hg $5d^{-1}$ photoelectrons. The solid curve is a relativistic random-phase approximation (RRPA) calculation from Refs. 8 and 9.

Fig. 7. Angular distribution asymmetry parameter of the Hg $4f^{-1}$ photoelectrons. The solid curve is an RRPA calculation from Ref. 9.

CORRELATION SATELLITES

The photoionization of He provides the simplest example of electron correlation in atomic physics. For photon energies above the second ionization limit of He(65.4 eV), it is possible to produce a He^+ ion in the ground state (1s) or in one of two excited (satellite) states (2s, 2p). We have studied the production of the n=2 satellites by the measurement of the partial cross section $\sigma(\varepsilon)$, the branching ratio to the ground ionic state, and the angular distribution asymmetry parameter $\beta(\varepsilon)$ as functions of photon energy, for the combination of the 2s and 2p final ionic states, which are effectively degenerate in a photoemission experiment. These studies were made with photon energies from near threshold to 90 eV, and are comprised of two distinct sets of data. The first set, off-resonance, was taken with photon energies from just above threshold to 69.5 eV and from 75 to 90 eV. The second set of data, on-resonance, was taken with photon energies (69.5-73 eV) capable of exciting members of a Rydberg series leading to the $He^+(n=3)$ ionization threshold at 73 eV. For both sets of measurements, the DATOF method allowed us to simultaneously determine the partial cross sections and asymmetry parameters for both the one-electron ionization to $He^+(n=1)$ and the simultaneous, two-electron ionization and excitation to $He^+(n=2)$.

In the off-resonance regions, the partial cross section and branching ratio (to the ground ionic state) measured show excellent agreement with previous experimental results.[10,11] The

off-resonance $He^+(n=2)$ asymmetry parameter, $\beta_{n=2}(\varepsilon)$, measured here, also shows good agreement with previous results above 75 eV photon energy (Fig. 8),[12] and has determined, for the first time, the behaviour of $\beta_{n=2}(\varepsilon)$ near threshold.

The asymmetry parameter measurable in this experiment, $\beta_{n=2}(\varepsilon)$, is an average of the asymmetry parameters for ionization to $He^+(2s)$ and $He^+(2p)$, weighted by the respective partial cross sections, as shown in Eq. (3).

$$\beta_{n=2}(\varepsilon) = \frac{\sigma_{2s}(\varepsilon)\beta_{2s} + \sigma_{2p}(\varepsilon)\beta_{2p}(\varepsilon)}{\sigma_{2s}(\varepsilon) + \sigma_{2p}(\varepsilon)} \qquad (3)$$

The value of β_{2s} is always two. Rearranging Eq. (3), we find an expression for the relative populations of $He^+(2p)$ and $He^+(2s)$;

$$R = \frac{\sigma_{2p}(\varepsilon)}{\sigma_{2s}(\varepsilon)} = \frac{2 - \beta_{n=2}(\varepsilon)}{\beta_{n=2}(\varepsilon) - \beta_{2p}(\varepsilon)} \cdot \qquad (4)$$

Thus, by measuring $\beta_{n=2}(\varepsilon)$ and using theoretical values for $\beta_{2p}(\varepsilon)$, the intensity ratio R of the excited ionic state can be determined. Fig. 8 shows two theoretical calculations of $\beta_{2p}(\varepsilon)$[13,14] as well as experimental[12] and theoretical[12] values for $\beta_{n=2}(\varepsilon)$. The solid circles represent the present data, which indicate that the value of $\beta_{n=2}(\varepsilon)$ approaches zero near threshold, in disagreement with the calculation of Bizau et al.[12] From Eq. (4), it is possible to calculate R, the ratio of the cross sections for production of $He^+(2p)$ to $He^+(2s)$, from the values of the satellite asymmetry parameter. This has been done, using $\beta_{2p}(\varepsilon)$ values calculated by Jacobs and Burke,[13] for both the present data and those of Bizau et al.[12] The results are shown in Fig. 9, where we see that the close-coupling theory of Jacobs and Burke[13] has the correct qualitative shape, in contrast to the indication from the previous data[12] that Chang's theory[14] is more correct.

In the resonance region, dramatic changes in the $He^+(n=2)$ partial cross section and asymmetry parameter were seen as functions of photon energy (see Figs. 10 and 11). This structure is attributed to the $He^*(3s3p)$ and $He^*(sp, 3n^+, n=4,5)$[15] autoionizing levels leading to the $He^+(n=3)$ ionization threshold. As discussed in Sec. II, it is possible to derive, from the cross section data, parameters describing these Fano profiles[4] in terms of the matrix elements governing the autoionization process. This has been done by Woodruff and Samson,[16] and the fit to their data is shown with the present results in Fig. 10. Interpretation of the on-resonance results for the asymmetry parameter, however, awaits further theoretical development of the behaviour of the angular distribution of photoelectrons from

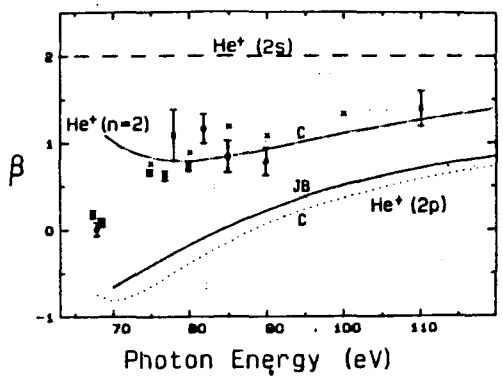

Fig. 8

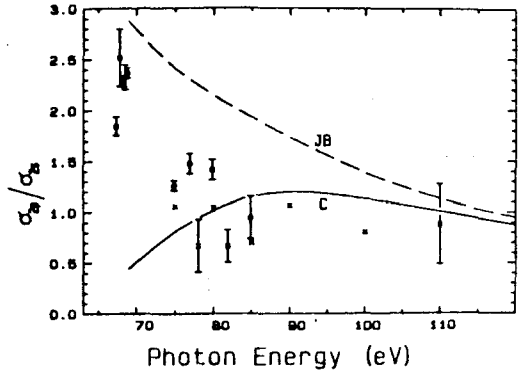

Fig. 9

Fig. 8. Angular distribution asymmetry parameter for $He^+(n=2)$ photoelectrons: • - present results; x - Ref. 12. Theoretical curves: (JB) - Jacobs and Burke, Ref. 13 and dotted curve (C) - Chang, Ref. 14 are calculations for $He^+(2p)$ only. The dot-dash curve (C) is a calculation of $He^+(n=2)$ by Bizau et al.[12]

Fig. 9. Ratio, R, of partial cross sections for photoionization to $He^+(2p)$ and $He^+(2s)$: • - present results; x - Ref. 12. Note that these values are calculated using values for $\beta_{2p}(\varepsilon)$ calculated in Ref. 13. Theoretical curves: (JB) - Ref. 13; (C) - Ref. 14.

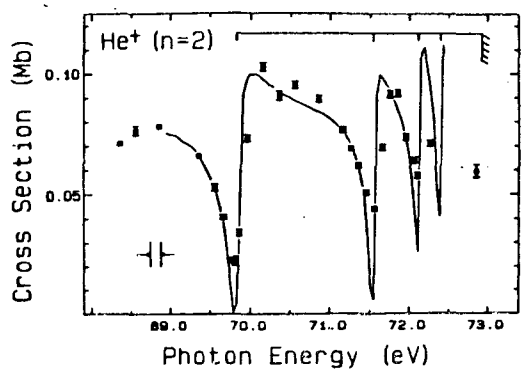

Fig. 10

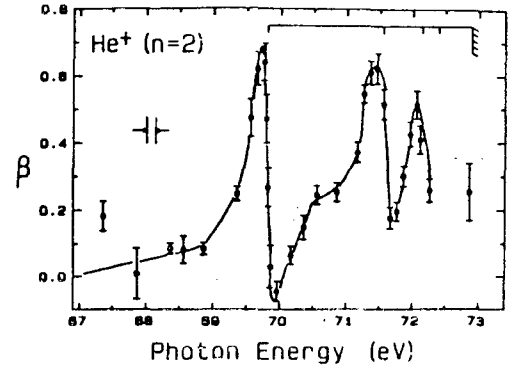

Fig. 11

Fig. 10. Partial cross section for photoionization to $He^+(n=2)$. The oscillations are due to the autoionizing states $He^+(3s3p)$ at 69.8 eV and $He^*(sp, 3n^+, n=4,5)$ at 71.55 and 72.13 eV. The solid curve is a fit to the data of Ref. 16.

Fig. 11. Angular distribution asymmetry parameter of the $He^+(n=2)$ photoelectrons. See caption of Fig. 10 for explanation. The solid curve is drawn only as a visual aid.

individual subshells in the vicinity of autoionization resonances.

After He the simplest and perhaps best understood satellite spectrum is that of Ne. The high resolution Al Kα spectrum of the Ne K-shell satellites[17] has been analyzed in detail using the sudden approximation and configuration interaction theory by Martin and Shirley.[18] The applicability of the sudden approximation greatly simplifies the analysis.

With the availability of the double-crystal monochromator at SSRL, our group has begun exploratory work on the threshold behavior of the Ne and Ar K-shell satellites. In the sudden approximation, the satellite to main line ratio should be constant while threshold effects may change this ratio. Preliminary experiments on Ne show a satellite to main line ratio below the sudden limit. The Ar K-shell spectrum, which has not been previously recorded, shows several satellite lines, the first of which increases in intensity by a factor of two relative to the main line between 25 and 85 eV kinetic energy.

We have also measured the asymmetry parameters and branching ratios of Ne(2s,2p) correlation satellites referenced to the 2s main line to further investigate electron correlation effects. The Ne 2s and 2p photo-peaks were used to calibrate the measurement of asymmetry parameters and correct the cross section data for the transmission of the 54.7° detector. The counting statistics were sufficient that satellite structure was observable. Figure 12 shows a TOF spectrum converted to photoelectron energy taken at 66.36 eV photon energy showing satellites derived from the configurations $2p^4ns$, $2p^4nd$, $2p^4np$ (S1,S2,S3,S4,S5), and the 2s line. Table I lists the configurations[19,20] and the comparable assignments given by Wuilleumier and Krause.[21] Fig. 13 shows the $\beta(\varepsilon)$'s for satellites S1, S3, S4, and S5. We observe that the $\beta(\varepsilon)$'s for S3, S4, and S5 follow the same general trend as $\beta(\varepsilon)$ for the Ne 2p main line. In contrast, S1

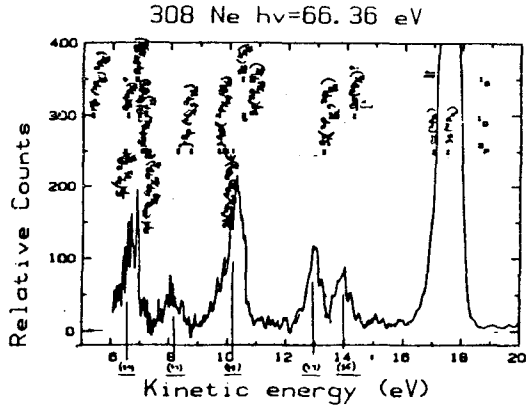

Wuilleumier Assignment	ε	Our Assignment	ε	ΔE		
1	60					
2	39					
3	37.97	S_1	37.51	303	$(^2p)3s$	$(^2p)4s^2r.^2p.^2p(^2p)3s^2p$
4	36.66	S_2	36.31	293	$(^2p)4s^2p.^2p$	
5	35.1					
6	34.04					
7	34.31	S_3	34.11	275	$(^1p)3p^2p.^2p.^2r$	$(^1s)3s^2s$
8	33.4					
9	32.24					
10	31.65	S_4	31.41	254	$(^2p)3p^2p$	
11	30.47	S_5	30.41	245	$(^2p)3p^4p$	$(^1p)3p^2p$
12	29.62					
25	26.1	2s	26.91	217		

Table I. The assignments and ionization thresholds referenced to Ne(I) given by Wuilleumier and our present results.

Fig. 12. Time-to-energy converted spectrum of Ne at a photon energy of 66.36 eV.

appears somewhat different. The asymptotic value of S1 does not agree well with the other three satellite peaks. This suggests that S1 contains $2p^4nd$ configurations mixed with $2p^4np$ and $2p^4ns$ configurations, while S3, S4, and S5 contain large $2p^4np$ admixtures with a smaller $2p^4ns$ contribution.

The branching ratios of satellites 1-5 are shown in Fig. 14. S3-S5 show a decrease in intensity at 61.5 ± 0.3 eV. Satellite 1 shows a weak minimum at ~ 74 eV. A preliminary explanation for the decrease observed in the branching ratio for S3 is that it is due to autoionization of a doubly-excited Rydberg level.

Equation (5) represents excitation to a resonant bound state. Equations (6a) and (6b) represent this state's subsequent autoionization.

$$(He)2s^2 2p^6 + h\nu \rightarrow Ne^* \qquad (5)$$

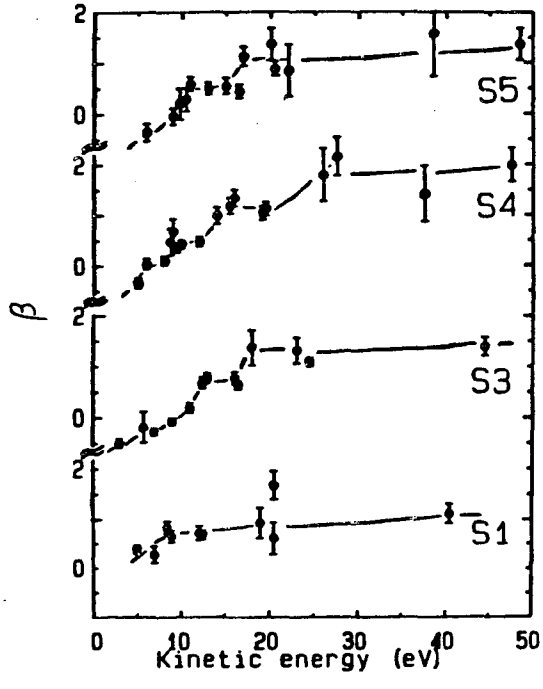

Fig. 13. Asymmetry parameters for satellites 1, 3, 4, and 5.

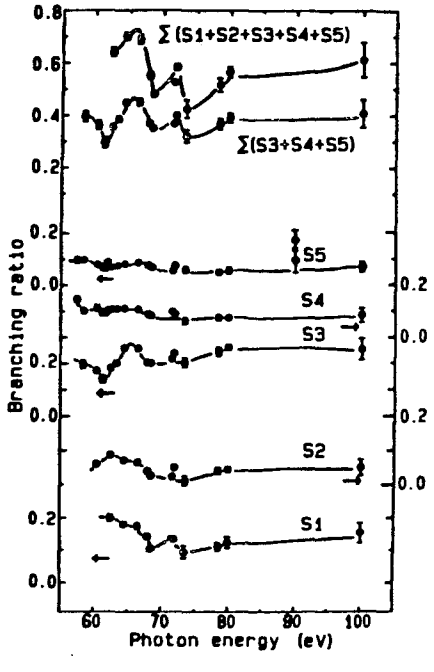

Fig. 14. Branching ratios of Ne satellites which are referenced to the $(2s)^{-1}$ core.

$$Ne^* \rightarrow (He)2s^2 2p^4 4s + e^- \qquad (6a)$$

$$Ne^* \rightarrow (He)2s^2 2p^4 4p + e^- \qquad (6b)$$

The occurrence of this resonant excitation could influence the intensity of S2 (Eq. (6b)). Further measurements must be performed to clarify the behavior of S3. Theoretical calculations including initial and final state configuration correlations and transitions to doubly-excited Rydberg levels of Ne(I) that predict the intensities and asymmetry parameters of Ne satellites would complement these experimental measurements.

K-SHELL EXCITATIONS OF SMALL MOLECULES

There is great interest in studying discrete and continuum transitions in the K-shells of small molecules for exploring absorption, potential barriers, and photoionization processes theoretically[22-25] and experimentally.[26-29] Shape resonances have been observed previously in photoabsorption and electron impact experiments.[26-29] In this paper we report the first observations of shape resonances in free molecules in the photoemission and Auger channels following core-level excitation. For the past two years, our group has measured K-shell asymmetry parameters $\beta(h\nu)$ and partial cross sections $\sigma(h\nu)$ for Auger and photoelectrons from the C(1s) shell in CO, CO_2, OCS, and CF_4, the O(1s) shell in CO and CO_2, and the N(1s) shell in N_2 and NO.

The excitation of the C K-shell in CO, CO_2, OCS, and CF_4 clearly demonstrates that the asymmetry parameters of KLL Auger and photoelectrons can be used to explore C(1s) discrete transitions, molecular shape resonances, and the influence of shape resonances on the KLL Auger decay process. Fig. 15 shows $\sigma(h\nu)$ and $\beta(h\nu)$ for the carbon KLL Auger peaks of CO. A discrete transition is responsible for the Auger resonance, clearly seen in the cross section at 287.3 eV. Dill et al.[30] have used the multiple-scattering method (MSM) to calculate the orientation parameter $\beta_m(h\nu)$ for $\sigma \rightarrow \pi$ discrete transitions. The excited $CO^*(^1\pi)$ molecule should orient perpendicular to the photon $\vec{E}$ vector following excitation. Note that β (287.3) is ~ 0. This may be a consequence of the experimental averaging over the KVV Auger transitions. At resonance, β is esssntially zero for the KVV Auger peaks in CO_2, OCS, and CF_4. $\beta_m(h\nu)$ is related to $\beta(h\nu)$ by a constant factor ($\mathcal{A}$) that is independent of the excitation energy and is only dependent on the dynamics of the Auger decay process as shown in the following equation

$$\beta(h\nu) = \beta_m(h\nu) * \mathcal{A} \qquad (7)$$

where $-1 \leq \beta_m(h\nu) \leq 2$ and $-1/2 \leq \mathcal{A} \leq 1$.[30]

Fig. 16 shows the C(1s) $\sigma(h\nu)$ and $\beta(h\nu)$ for CO. The solid curve is the MSM calculation performed by Dill et al.[22] and the dashed curve pictured with our results (•) for the C(1s) $\beta(h\nu)$ is the MSM calculation of Grimm.[23] We show excellent agreement with Dill et al.[30] for the shape of $\beta(h\nu)$ as a function of photon energy, but the minimum occurs between the two calculations. The manifestation of the continuum shape resonance ($\sigma \rightarrow \sigma^*$) results in a minimum for the $\beta(h\nu)$ of the C(1s) photoelectron. The $\sigma(h\nu)$ clearly shows the shape resonance as a broad peak centered at 305.0 eV. We have excellent agreement with the Stieltjes-Tchebycheff calculation of Padial et al.[24] Our relative cross sections for the C(1s) photoelectron were scaled to Kay et al.[26] electron-ion coincidence experimental cross sections to yield C(1s) absolute partial cross sections. An expansion of the C(KVV) Auger cross section over the shape resonance region demonstrates that the Auger cross section is influenced by the continuum resonance.

The solid line pictured in Fig. 15 with the C(KLL) Auger $\beta(h\nu)$ is the calculation of $\beta_m(h\nu)$ by Dill et al.[30] Our results show less variation than their calculation.

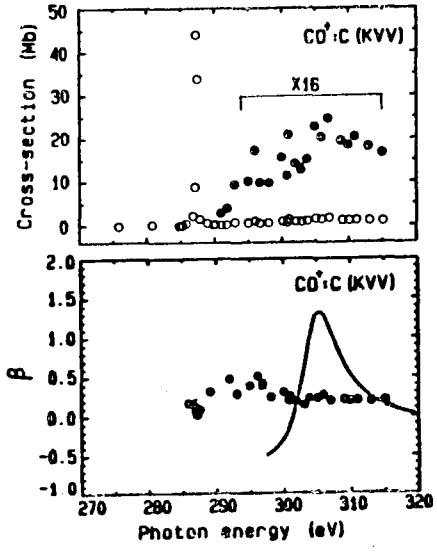

Fig. 15

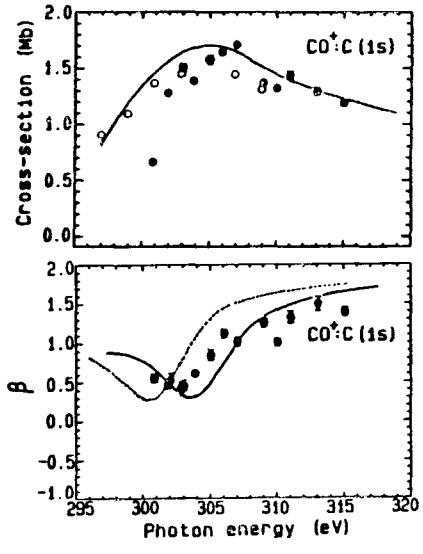

Fig. 16

Fig. 15. Partial cross section and angular distribution asymmetry parameter for C(KVV) Auger electrons from CO.

Fig. 16. Partial cross section and angular distribution asymmetry parameter for C(1s) photoelectrons from CO.

As a comparison, Fig. 17 shows the $\beta(h\nu)$ for the C(1s) photoelectron in CO_2. Here the shape resonance is ~ 20 eV broad and located more than 1 Rydberg from threshold. The dashed curve in Fig. 17 is a calculation by Grimm[23] and the solid curve is a Hartree-Fock calculation by Lucchese and McKoy.[25]

The O K-shell is also predicted to have shape resonances and discrete transition resonances. Most of our O K-shell results were obtained from the second order light present during the measurement of the C K-shell systems. Unfortunately, the shape resonance region was not done in detail. One can infer from our data that the O(1s) shape resonance is present. Fig. 18 shows the $\sigma(h\nu)$ and $\beta(h\nu)$ of the O(1s) photoelectron of CO. The O(1s) data were scaled such that the maximum in the O(1s) cross section was 2/3 that of the C(1s) cross section. The solid curve is a calculation by Padial et al.[26] There are data missing for the true maximum in the cross section at the O(1s) shape resonance, but because the cross section does not have a maximum at threshold, we can infer that a centrifugal barrier is present as the O(1s) photoelectron scatters through the molecular potential in CO.

Our $\beta(h\nu)$ measurements, also shown in Fig. 18, cannot be used to confirm if the theory of Grimm[23] (solid curve) or that of Dill et al.[22] (dashed curve) is more capable of predicting the asymmetry parameter. More work is necessary for any strong conclusions.

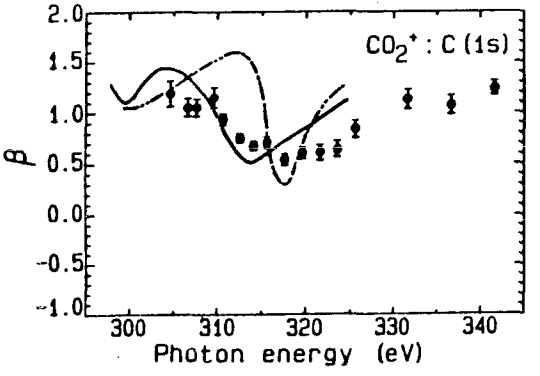

Fig. 17

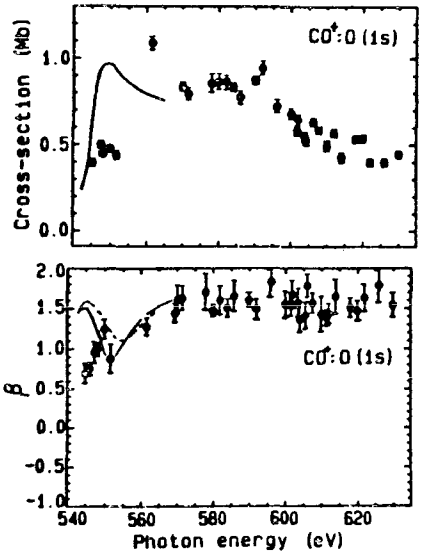

Fig. 18

Fig. 17. Angular distribution asymmetry parameter for C(1s) photoelectrons from CO_2.

Fig. 18. Partial cross section and angular distribution asymmetry parameter for O(1s) photoelectrons from CO.

In addition to the C and O K-shell measurements, we have measured partial cross sections and asymmetry parameters for photoemission and Auger electron emission from the N K-shell in N_2 and NO. Similar effects to those seen in the C K-edge experiments are apparent. One significant conclusion is that the σ shape resonance above threshold produces a much larger effect in N_2 than NO, despite the relative similarity of the two molecules.

INNER-VALENCE STUDIES

Recent measurements[31] by this group have confirmed the predicted oscillatory nature of the asymmetry parameter $\beta(\varepsilon)$ for the Xe 4d subshell. The behaviour seen is primarily due to non-relativistic, one-electron effects such as the variation of Coulomb phase shifts in outgoing photoelectron channels and the change in sign of radial matrix elements which occurs at a Cooper minimum. In the past few months, we undertook a similar experiment on methyl iodide (CH_3I) as a molecular analog of atomic Xe. We find that $\beta(\varepsilon)$ for the I 4d subshell in CH_3I exhibits almost identical behaviour to $\beta(\varepsilon)$ for the Xe 4d subshell over a wide photon energy range. We conclude from this that the 4d subshell on the iodine atom in CH_3I is primarily atomic and that the methyl group has little interaction with the outgoing photoelectron waves.

CONCLUSION

The last few years have seen the development and growth of a valuable technique in the study of the electronic properties of free atoms and molecules. The DATOF method has proven useful in the study of such diverse phenomena in photoelectron spectroscopy as electron correlation, autoionization, shape resonances and relativistic effects in a wide variety of atomic and molecular systems. We have provided a brief summary of some of the more unique and interesting results obtained recently by our group.

REFERENCES

*This work was supported by the Director, Office of Energy Research, Office of Basic Energy Sciences, Chemical Sciences Division of the U.S. Department of Energy under Contract No. DE-AC03-76SF00098. It was performed at the Stanford Synchrotron Radiation Laboratory, which is supported by the NSF through the Division of Materials Research.

†National Bureau of Standards, Washington, DC 20234.

1. M.G. White, R.A. Rosenberg, G. Gabor, E.D. Poliakoff, G. Thornton, S.H. Southworth, and D.A. Shirley, Rev. Sci. Instrum., 50, 1268 (1979).

2. S.H. Southworth, C.M. Truesdale, P.H. Kobrin, D.W. Lindle, W.D. Brewer, and D.A. Shirley, J. Chem. Phys. 76, 143 (1982).
3. R.A. Rosenberg, M.G. White, G. Thornton, and D.A. Shirley, Phys. Rev. Lett., 43, 1384 (1979).
4. U. Fano, Phys. Rev., 124, 1866 (1961).
5. A.F. Starace, Phys. Rev. A 16, 231 (1977).
6. L.C. Davis and L.A. Feldkamp, Phys. Rev. B 23, 6239 (1981).
7. P.H. Kobrin, U. Becker, S.H. Southworth, C.M. Truesdale, D.W. Lindle, and D.A. Shirley, Phys. Rev. A 26, 842 (1982).
8. W.R. Johnson, V. Radojević, P. Deshmukh, and K.T. Cheng, Phys. Rev. A 25, 337 (1982).
9. V. Radojević and W.R. Johnson, private communication.
10. M.O. Krause and F. Wuilleumier, J. Phys. B 5, L143 (1972). F. Wuilleumier, M.Y. Adam, N. Sandner, and V. Schmidt, J. Physique-Lett., 41, L373 (1980).
11. P.R. Woodruff and J.A.R. Samson, Phys. Rev. Lett., 45, 110 (1980).
12. J.M. Bizau, F. Wuilleumier, P. Dhez, D.L. Ederer, T.N. Chang, S. Krummacher, and V. Schmidt, Phys. Rev. Lett. 48, 588 (1982).
13. V.L. Jacobs and P,G. Burke, J. Phys. B 5, L67 (1972).
14. T.N. Chang, J. Phys. B 13, L551 (1980).
15. R.P. Madden and K. Codling, Astrophys. J., 141, 364 (1965).
16. P.R. Woodruff and J.A.R. Samson, Phys. Rev. A 25, 848 (1982).
17. U. Gelius, J. Elect. Spect., 5, 985 (1974).
18. R.L. Martin and D.A. Shirley, Phys. Rev. A 13, 1475 (1976).
19. C.E. Moore, Atomic Energy Levels, National Bureau of Standards 457, 1949.
20. W. Persson, Physica Scripta, 3, 133 (1971).
21. F. Wuilleumier and M.O. Krause, Phys. Rev. A 10, 242 (1974).
22. J.L. Dehmer and D. Dill, Phys. Rev. Lett. 35, 213 (1975); J.L. Dehmer and D. Dill, J. Chem. Phys. 65, 5327 (1976); D. Dill, S. Wallace, J. Siegel, and J.L. Dehmer, Phys. Rev. Lett. 42, 411 (1979).
23. F.A. Grimm, Chem. Phys. 53, 71 (1980).
24. N. Padial, G. Csanak, B.V. McKoy, and P.W. Langhoff, J. Chem. Phys. 69, 2962 (1978).
25. R.R. Lucchese and B.V. McKoy, to be published.
26. R.B. Kay, Ph.E. Van der Leeuw, and U.J. Van der Wiel, J. Phys. B 10, 2513 (1973).
27. M. Tronc, G.C. King, R.C. Bradford, and F.H. Read, J. Phys. B 9, L555 (1976).
28. A. Hamnett, W. Stall, and C.E. Brion, J. Elect. Spect., 8, 367 (1976).
29. G.R. Wight, C.E. Brion, and M.J. Van der Wiel, J. Electr. Spectr., 1, 457 (1972).
30. D. Dill, J.R. Swanson, S. Wallace, and J.L. Dehmer, Phys. Rev. Lett. 45, 1393 (1980).
31. S.H. Southworth, P.H. Kobrin, C.M. Truesdale, D.W. Lindle, S. Owaki, and D.A. Shirley, Phys. Rev. A 24, 2257 (1981).